ELSEVIER

Journal of Contaminant Hydrology 16 (1994) 203–234

JOURNAL OF
Contaminant
Hydrology

An improved sharp-interface model for assessing NAPL contamination and remediation of groundwater systems

P.S. Huyakorn, Yu-Shu Wu, N.S. Park

HydroGeoLogic, Inc., 1165 Herndon Parkway, Suite 900, Herndon, VA 22070, USA

(Received October 25, 1993; revision accepted April 8, 1994)

Abstract

A numerical model is presented for areal analyses of the three-dimensional (3-D) flow behavior of non-aqueous-phase liquids (NAPL's) in groundwater systems. The model is designed for specific application to chemical or petroleum spills and leaks, and remedial design and evaluation of a NAPL-contaminated site. The mathematical formulation is based on vertical integration of the 3-D two-phase flow equations and incorporation of the modified concept of gravity-segregated vertical equilibrium (GSVE) which yields sharp interfaces separating the zones of mobile NAPL and groundwater. History-dependent pseudo constitutive relations are developed for LNAPL's and DNAPL's (light and dense NAPL's) scenarios taking into account the effects of residual saturations. Owing to the sharp-interface assumption, the soil capillary pressure and relative permeability curves are not needed in the evaluation of pseudo functions. Efficient and mass-conservative nonlinear numerical techniques are adopted for solving the governing equations and treating practical boundary conditions which include injection and recovery wells and trenches. Simulation and application examples are provided to demonstrate verification and utility of the model. Numerical results obtained using the sharp-interface modeling approach are compared with analytical solutions and rigorous multiphase numerical solutions that account for vertical flow components and capillary effects. The verification results show the validity of the GSVE modeling assumptions and accuracy of the proposed formulation and computational schemes in predicting the NAPL recovery. The numerical study also indicates that the present model is highly efficient and is thus suitable for preliminary analyses of site-specific problems with limited data and personal computer resources.

1. Introduction

The release and subsurface migration of non-aqueous-phase liquids (NAPL's) such as oily wastes, petroleum products and industrial chemicals have caused serious

SSDI 0169-7722(94)0000-0

groundwater contamination problems throughout the U.S.A. Modeling assessments of contaminant migration and remedial options are becoming crucial due to the increased necessity to address and mitigate the environmental problems. A number of numerical models have been documented which describe the simultaneous flow of groundwater and NAPL in unconfined aquifer systems. However, most field-scale simulations performed to date have been limited to cross-sectional analyses involving a vertical slice through unsaturated and/or saturated zones (Abriola and Pinder, 1985; Faust, 1985; Forsyth, 1988, 1991; Kaluarachchi and Parker, 1989). Such two-dimensional (2-D) models do not provide adequate treatment of many field situations which involve areal variations of aquifer properties and/or dominant horizontal transverse flow components due to, for example, implementation of remedial schemes. Three-dimensional (3-D) multiphase flow models have been described recently by Faust et al. (1989), Letniowski and Forsyth (1991), and Huyakorn et al. (1992). However, the computational burden of fully 3-D analyses still imposes severe constraints on their application.

An alternative simulation approach to complex field problems is via the use of an areal model based on vertical integration of the 3-D multiphase flow equations under a vertical equilibrium (VE) or hydrostatic assumption. Such an approach is widely known in the petroleum reservoir modeling literature and is based on the original works of Coats et al. (1967, 1971), and Martin (1968). The VE modeling approach offers several advantages which include reducing the spatial dimensionality and non-linearity of the problem. Thus, savings in computational resources can be substantial. Furthermore, input data requirements for rock or soil capillary pressure and relative permeability curves may be removed by using an additional assumption of gravity segregation which yields a sharp interface separating the two immiscible liquids. However, the VE model has certain limitations in that it cannot predict the vertical movement and the detailed spatial distributions of fluids. The practical applicability of the model depends upon the rapidity with which perturbation from equilibrium in the vertical direction dissipates as compared with the rate of movement in the horizontal directions. The VE model can be employed successfully only under the appropriate field conditions.

Several VE numerical models have been proposed for areal simulation of NAPL migration (Hochmuth and Sunada, 1985; Charbenau et al., 1989; Kaluarachchi et al., 1990). However, these models are applicable only to light non-aqueous-phase liquids (LNAPL's) and not to dense non-aqueous-phase liquids (DNAPL's). Furthermore, there are other shortcomings in the model formulations. The models presented by Hochmuth and Sunada (1985), and Charbenau et al. (1989) are based on sharp-interface formulations that incorporate residual saturations in the storage terms of the equations. However, the effects of the storage terms vanish when steady-state conditions are reached. Therefore, situations where the NAPL mass becomes immobile cannot be predicted. The model presented by Kaluarachchi et al. (1990) uses a more sophisticated formulation that accounts for the effects of capillary pressure on saturation distribution. However, there are some limitations in the model (see Parker and Lenhard, 1989). For instance, the residual oil saturation is regarded as zero and the VE condition is assumed not only in the liquid-saturated

zones but also in the overlying vadose zone. Physically, vertical equilibrium implies uniform vertical distributions of water and NAPL potentials. In the vadose zone, however, the vertical gradients of the fluid potentials are usually significant because of the impact of water infiltration and the tendency of the NAPL to move downward toward the water table. Consequently, the VE assumption may be invalid.

Similarly, a number of sharp-interface models have been used to study saltwater intrusion problems in which freshwater and saltwater are simulated as immiscible fluids separated by a sharp interface (Sa da Costa and Wilson, 1979; Essaid, 1990). The flow governing equations are also based on vertical integration of the 3-D mass-balance equations for two fluids and coupled through the interface continuity condition for flux and pressure. However, these saltwater interface models are generally not applicable to NAPL movement problems unless both residual water saturation and residual NAPL saturation are assumed to be zero in aquifers.

The objective of the present study is three-fold: (1) to present VE model formulations and numerical solution techniques that improve the previous works; (2) to verify the mathematical formulations and numerical schemes for accuracy, stability and ability to simulate different field conditions; and (3) to demonstrate the practical utility of the proposed formulations.

Robust and efficient numerical techniques have been incorporated in our proposed model to enable practical simulations of site-specific field problems on personal computers and workstations. The governing equations are discretized using a modified Galerkin finite-element method with an influence coefficient scheme for element matrix computation thereby avoiding numerical integration. Nonlinearities are treated using the Newton–Raphson technique. The convergence and efficiency of the overall nonlinear solution procedure are enhanced by an advanced time stepping control scheme which takes the full advantage of the Newton–Raphson scheme. Simulation examples are presented to verify the numerical scheme implemented and the model assumptions used. In addition, the present model has been used to simulate the crude-oil lens movement and distribution at the site of a crude-oil spill near Bemidji, Minnesota, U.S.A. Reasonable agreement has been obtained between the sharp-interface model predictions of the oil lens, the observed data, and the multiphase simulation results. The significance of the sharp-interface modeling approach is examined in view of data requirements and reliability of simulation results.

2. Vertical equilibrium (VE) concept

The VE concept evolves from the petroleum reservoir engineering literature (Coats et al., 1967, 1971; Martin, 1968; Aziz and Settari, 1979; Thomas, 1982). The concept has been used to allow areal simulation of 3-D reservoir performance. Reservoirs are said to be in a VE state when the pressure in each fluid phase varies hydrostatically along any traverse line perpendicular to the underlying and overlying formation surfaces. For most reservoirs whose formation surfaces are relatively flat, the traverse line is essentially vertical and the ratio of thickness to maximum horizontal distance is usually small.

In mathematical terms, the VE assumption for a two-phase system may be expressed as:

$$\frac{\partial \Phi_\ell}{\partial z} = 0 \qquad (\ell = \mathrm{w},\ \mathrm{n}) \tag{1}$$

where Φ_ℓ is the fluid potential function for the ℓ-phase (w = water, n = NAPL); z is the upward vertical coordinate; and w and n denote the aqueous and non-aqueous liquid phases, respectively. The fluid potential function is defined as (Thomas, 1982):

$$\Phi_\ell = p_\ell + \rho_\ell g z \tag{2}$$

where p_ℓ and ρ_ℓ are the fluid pressure and density, respectively; and g is the gravitational constant.

Two types of VE model may be conceptualized. These are referred to as the gravity–capillary vertical equilibrium (GCVE) and the gravity-segregated vertical equilibrium (GSVE) models. Both conceptual models are described below.

2.1. Gravity–capillary vertical equilibrium (GCVE)

The GCVE model considers vertical equilibrium as a result of a balance of gravity and capillary forces in the dip-normal direction of the reservoir (assumed here to correspond to the vertical direction). The existence of capillary transition zone of appreciable thickness is taken into account. If the state of GCVE is attained, then knowledge of the value of capillary pressure at any point on the reference surface establishes the variation of capillary pressure along the dip-normal line through that point (Coats et al., 1967). If the positive z-coordinate in the vertically upward direction, the mathematical equivalence of this statement may be expressed as (Martin, 1968):

$$p_{\mathrm{w}}(x,y,z) = p_{\mathrm{w}}^*(x,y) - g\cos\alpha \int_{z^*}^{z} \rho_{\mathrm{w}}\,\mathrm{d}z \tag{3a}$$

$$p_{\mathrm{n}}(x,y,z) = p_{\mathrm{n}}^*(x,y) - g\cos\alpha \int_{z^*}^{z} \rho_{n}\,\mathrm{d}z \tag{3b}$$

where x and y are areal coordinates; $p^*(x,y)$ is the fluid pressure at a point on the reference surface; α is the dip angle (assumed to be zero); and z^* is the elevation of the reference point above the datum plane. Since ρ_{n} and ρ_{w} are essentially constant, Eqs. 3a and 3b can be easily integrated and combined to give:

$$p_{\mathrm{c}}(x,y,z) = p_{\mathrm{c}}^*(x,y) - (\rho_{\mathrm{n}} - \rho_{\mathrm{w}})g(z - z^*) \tag{4}$$

where the capillary pressures are:

$$p_{\mathrm{c}}(x,y,z) = p_{\mathrm{n}}(x,y,z) - p_{\mathrm{w}}(x,y,z) \tag{5a}$$

and

$$p_{\mathrm{c}}^*(x,y) = p_{\mathrm{n}}^*(x,y) - p_{\mathrm{w}}^*(x,y) \tag{5b}$$

2.2. Gravity-segregated vertical equilibrium (GSVE)

The GSVE model, which is formulated in this paper, regards capillary forces to be insignificant as compared to gravitational forces. Consequently, the latter are the driving forces toward equilibrated (segregated) vertical fluid distributions (i.e. the fluids are segregated). The model assumes that the capillary transition zone is very thin and may be approximated by an abrupt change (sharp interface). The interface corresponds to the surface of direct contact between the two fluids. At the interface we let $z = Z_c$ and impose the condition that $p_w(x, y, Z_c) = p_n(x, y, Z_c)$. Eqs. 3a and 3b are thus evaluated at $z = Z_c$ and combined to give:

$$\bar{p}_c = (\rho_w - \rho_n) g (z^* - Z_c) \tag{6}$$

In view of the fact that the real capillary pressure is assumed to be zero in the GSVE model, $\bar{p}_c(x, y)$ is regarded as the pseudo-capillary pressure. Note that $\bar{p}_c$ is a pseudo physical quantity because it has nothing to do with the actual rock or soil properties.

3. Vertically integrated flow equations

The VE concept has been successfully applied to petroleum reservoir engineering problems involving confined reservoirs with no-flow boundary conditions at the overlying and underlying formation surfaces. The concept may be adapted to NAPL– groundwater contamination problems in unconfined and leaky or nonleaky confined aquifers. In developing the governing equations for areal sharp-interface flow in such aquifers, we assume that near GSVE conditions occur only in the saturated zone of the groundwater system.

The governing equations of the GSVE model can be derived by performing vertical integration of 3-D two-phase flow equations from the aquifer base Z_B to the top surface Z_T. The resulting vertically integrated equations for horizontal confined and unconfined aquifers under GSVE may be written in the form:

$$\frac{\partial}{\partial x}\left[\bar{k}_x \tau_{\ell x} \frac{\partial \Phi_\ell}{\partial x}\right] + \frac{\partial}{\partial y}\left[\bar{k}_y \tau_{\ell y} \frac{\partial \Phi \ell}{\partial y}\right] = \frac{\partial}{\partial t}(b \rho_\ell \bar{\phi} \bar{S}_\ell) - \dot{M}_\ell \qquad (\ell = \mathrm{w},\ \mathrm{n}) \tag{7}$$

$$\bar{k}_i = \frac{1}{b} \int_{Z_B}^{Z_T} k_i(z)\,\mathrm{d}z \qquad (i = x,\ y) \tag{8}$$

$$\tau_{\ell i} = b \bar{k}_{r\ell i} \rho_\ell / \mu_\ell \qquad (i = x, y) \tag{9}$$

$$\bar{k}_{r\ell i} = \frac{\displaystyle\int_{Z_B}^{Z_T} k_i(z) k_{r\ell}(z)\,\mathrm{d}z}{\displaystyle\int_{Z_B}^{Z_T} k_i(z)\,\mathrm{d}z} \qquad (i = x,\ y) \tag{10}$$

$$\overline{\phi} = \frac{1}{b}\int_{Z_B}^{Z_T} \phi(z)\mathrm{d}z \tag{11}$$

Note that k_i is the intrinsic permeability; $k_{r\ell}$ is the relative permeability of phase ℓ; b is the

$$\overline{S}_\ell = \frac{\int_{Z_B}^{Z_T} \phi(z) S_\ell(z)\mathrm{d}z}{\int_{Z_B}^{Z_T} \phi(z)\mathrm{d}z} \tag{12}$$

liquid-saturated thickness ($b = Z_T - Z_B$); ϕ is the effective porosity; μ_ℓ is the dynamic viscosity of phase ℓ; S_ℓ is the saturation of phase ℓ; the overbar denotes vertical averaging; and $\dot{M}_\ell$ is the net fluid mass flux term resulting from such factors as well pumping or injection, NAPL sources, groundwater recharge and aquitard leakage. It should be noted that the free-surface condition (Bear, 1972) has been used to approximate the liquid table in deriving the above equations for unconfined aquifers.

Eq. 7 is supplemented by the following relations:

$$\overline{S}_w + \overline{S}_n = 1 \tag{13}$$

$$\Phi_n = \Phi_w + \overline{p}_c - g(\rho_w - \rho_n)Z_B \tag{14}$$

$$\overline{k}_{r\ell} = \overline{k}_{r\ell}(\overline{S}_w, Z_D) \tag{15}$$

$$\overline{p}_c = \overline{p}_c(\overline{S}_w, Z_D) \tag{16}$$

where $\overline{p}_c$ and $\overline{k}_{r\ell}$ are the pseudo-capillary and pseudo relative permeability functions, respectively. In general, these functions are dependent on not only $\overline{S}_w$ (or $\overline{S}_n$) but also a second parameter Z_D that reflects the history of NAPL contamination as will be shown in the next section.

4. Pseudo constitutive relations

In handling the vertically integrated flow equations for both confined and unconfined aquifers, the pseudo functions of capillary pressure and relative permeabilities are needed to relate the primary variables and determine flow mobility terms. These pseudo functions depend on whether the NAPL is lighter or denser than water, and also on the history of NAPL contamination. The latter dependency needs to be taken into account in order to properly track the residual NAPL mass in the groundwater system. Both cases of LNAPL's and DNAPL's are treated below.

4.1. LNAPL *contaminant*

Consider a single vertical soil column overlying a specified nodal point. Under the

GSVE conditions, the LNAPL lens floats on the water table. The initial location of the interface is at $z = Z_{ci}$, and the saturation distributions are as shown in Fig. 1a, where S_{wr} is the residual (irreducible) water saturation. The initial value of vertically averaged water saturation, $\overline{S}_{wi}$, is given by:

$$\overline{S}_{wi} = [S_{wr}(Z_T - Z_{ci}) + (Z_{ci} - Z_B)]/b \tag{17}$$

At a later time, t_1, the LNAPL–water interface declines to a lower position, Z_c, as shown in Fig. 1b. In determining the saturation profiles, it is convenient to define Z_{min} as the minimum value of Z_c up to the previous time (t_k):

$$Z_D = Z_{min} = \text{Min}[Z_c(t)] \qquad \forall t \leqslant t_k \tag{18}$$

Note that Z_D or Z_{min} is the history-dependent parameter.

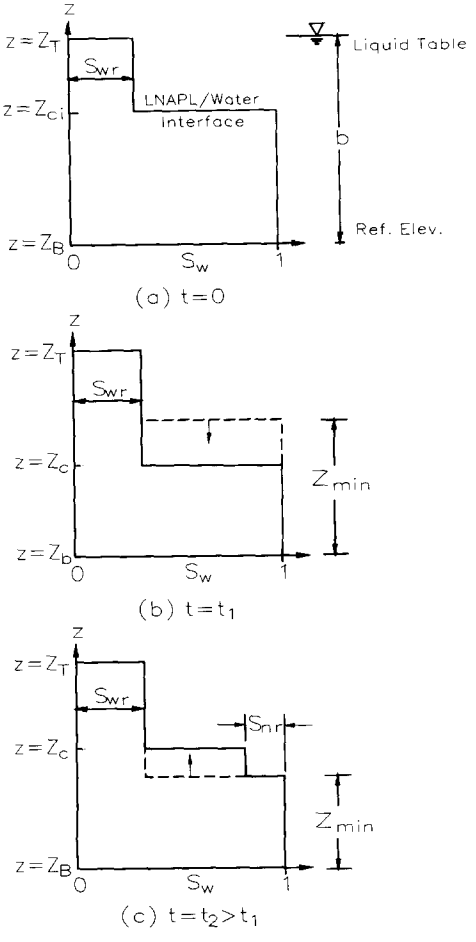

Fig. 1. Distributions of water and LNAPL under GSVE conditions.

When $Z_c \leqslant Z_{min}$, the vertically average water saturation is given by (Fig. 1b):

$$\bar{S}_w = [S_{wr}(Z_T - Z_c) + (Z_c - Z_B)]/b \tag{19}$$

where S_{wr} is the residual water saturation.

At the next time level, t_2, the interface rises as shown in Fig. 1c. In this case, $Z_c > Z_{min}$ and $\bar{S}_w$ is determined from:

$$\bar{S}[S_{wr}(Z_T - Z_c) + (1 - S_{nr})(Z_c - Z_{min}) + (Z_{min} - Z_B)]/b \tag{20}$$

where S_{nr} is the residual LNAPL saturation.

By choosing the elevation Z_B as the reference elevation and letting the corresponding pseudo-capillary pressure be $\bar{p}_c(x, y)$, one obtains from Eq. 6 the following expression:

$$\bar{p}_c = (\rho_w - \rho_n)g(Z_B - Z_c) \tag{21}$$

Combination of Eq. 21 with Eqs. 19 and 20 gives:

$$\bar{p}_c = -\frac{(\rho_w - \rho_n)gb(\bar{S}_w - S_{wr})}{1 - S_{wr}} \qquad \text{for} \quad Z_c \leqslant Z_{min} \tag{22}$$

$$\bar{p}_c = \frac{(\rho_w - \rho_n)g[(Z_{min} - Z_B)S_{nr} - b(\bar{S}_w - S_{wr})]}{1 - S_{wr} - S_{nr}} \qquad \text{for} \quad Z_c > Z_{min} \tag{23}$$

The pseudo relative permeability to water can normally be evaluated using Eq. 10. Under phase gravity-segregated conditions, however, $k_{rw} = 1$ or k^*_{rw} in the mobile water zone, and $k_{rw} = 0$ in the mobile NAPL zone. Then it turns out:

$$\bar{k}_{rw} = (Z_c - Z_B)/b \qquad \text{for} \quad Z_c \leqslant Z_{min} \tag{24}$$

and

$$\bar{k}_{rw} = [(Z_c - Z_{min})k^*_{rw} + (Z_{min} - Z_B)]/b \qquad \text{for} \quad Z_c > Z_{min} \tag{25}$$

where k^*_{rw} is the relative permeability to water at residual NAPL saturation ($S_n = S_{nr}$).

Using Eqs. 19 and 20 to eliminate Z_c in Eqs. 24 and 25, we can express $\bar{k}_{rw}$ as functions of $\bar{S}_w$ as follows:

$$\bar{k}_{rw} = \frac{\bar{S}_w - S_{wr}}{1 - S_{wr}} \qquad \text{for} \quad \bar{S}_w \leqslant \bar{S}_{wmin} \tag{26}$$

$$\bar{k}_{rw} = \frac{\bar{S}_w k^*_{rw}}{1 - S_{wr} - S_{nr}} - \left[\frac{S_{wr}(Z_T - Z_{min}) + (Z_{min} - Z_B)}{b(1 - S_{wr} - S_{nr})}\right] k^*_{rw} + \frac{(Z_{min} - Z_B)(1 - S_{wr} - S_{nr})}{b(1 - S_{wr} - S_{nr})} \qquad \text{for} \quad \bar{S}_w > \bar{S}_{wmin} \tag{27}$$

where $\bar{S}_{wmin}$ is the minimum vertically average water saturation, defined as:

$$\bar{S}_{wmin} = [S_{wr}(Z_T - Z_{min}) + (Z_{min} - Z_B)]/b \tag{28}$$

Similarly, the pseudo functions of relative permeability to NAPL may be

obtained as:

$$\bar{k}_{rn} = \frac{k^*_{rn}}{1 - S_{wr}}(1 - \bar{S}_w) \qquad \text{for} \quad \bar{S}_w \leqslant \bar{S}_{wmin} \tag{29}$$

and

$$\bar{k}_{rn} = \frac{k^*_{rn}}{1 - S_{wr} - S_{nr}}\left[1 - \frac{S_{nr}(Z_T - Z_{min})}{b} - \bar{S}_w\right] \qquad \text{for} \quad \bar{S}_w > \bar{S}_{wmin} \tag{30}$$

where k^*_{rn} is the relative permeability to NAPL at $S_w = S_{wr}$.

At each time level, we need to determine the location of the interface (Z_c) in order to determine the vertical profiles of water and NAPL saturations. The required expressions for Z_c are given by:

$$Z_c = \frac{b\bar{S}_w - S_{wr}Z_T + Z_B}{1 - S_{wr}} \qquad \text{for} \quad \bar{S}_w \leqslant \bar{S}_{wmin} \tag{31}$$

and

$$Z_c = \frac{b\bar{S}_w - S_{wr}Z_T - S_{nr}Z_{min} + Z_B}{1 - S_{wr} - S_{nr}} \qquad \text{for} \quad \bar{S}_w > \bar{S}_{wmin} \tag{32}$$

4.2. DNAPL *contaminant*

Under GSVE conditions, the DNAPL mass pools on the aquifer base. The initial location of the interface is at Z_{ci} and the saturation distributions are as shown in Fig. 2a. The initial vertically averaged water saturation is given by:

$$\bar{S}_{wi} = [(Z_T - Z_c) + S_{wr}(Z_{ci} - Z_B)]/b \tag{33}$$

At a later time t_1, the interface rises to a new position, Z_c, as shown in Fig. 2b. In determining the saturation profiles, we need to introduce Z_{max} as the maximum value of Z_c up to the previous time (t_k):

$$Z_D = Z_{max} = \text{Max}[Z_c(t)] \qquad \forall t \leqslant t_k \tag{34}$$

Note that Z_{max} is now the history-dependent parameter. Z_{max} corresponds to Z_{min}, which was introduced previously for the case of LNAPL contamination. It can readily be shown that the influence of Z_{max} (or Z_{min}) on the pseudo functions diminishes if S_{nr} is set to zero.

We now proceed with the derivation of the pseudo functions for the general case where S_{nr} is greater than zero. Initially,

$$Z_c = Z_{ci} \tag{35}$$

It follows from Fig. 2b that when $Z_c > Z_{max}$, the vertically averaged water saturation, $\bar{S}_w$, is given by:

$$S_w = [(Z_T - Z_c) + S_{wr}(Z_c - Z_B)]/b \tag{36}$$

At the next time level, t_2, the interface declines as shown in Fig. 2c. In this case

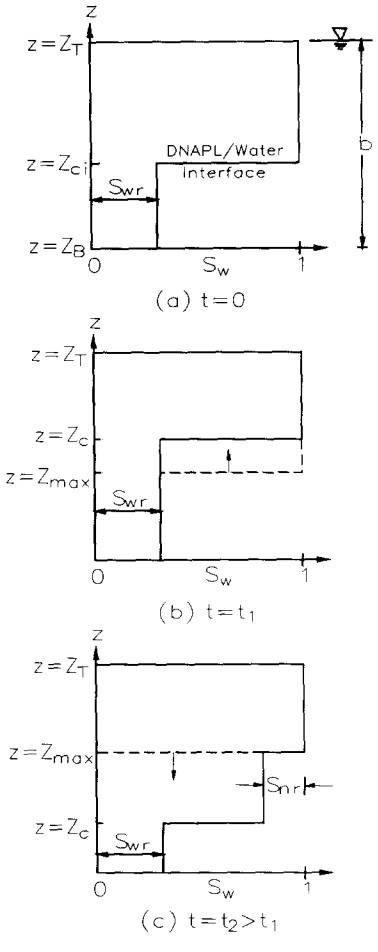

Fig. 2. Distributions of water and DNAPL under GSVE conditions.

$Z_c < Z_{max}$ and $\overline{S}_w$ is given by:

$$\overline{S}_w = [(Z_T - Z_{max}) + (1 - S_{nr})(Z_{max} - Z_c) + S_{wr}(Z_c - Z_B)]/b \tag{37}$$

In a similar manner to the LNAPL scenario, the pseudo-capillary pressure can be expressed in terms of $\overline{S}_w$ as follows:

$$\overline{p}_c = -\frac{(\rho_w - \rho_n)gb(1 - \overline{S}_w)}{(1 - S_{wr})} \qquad \text{for} \qquad Z_c \leqslant Z_{max} \tag{38}$$

and

$$\overline{p}_c \frac{(\rho_w - \rho_n)g[S_{nr}(Z_{max} - Z_B) - b(1 - \overline{S}_w)]}{1 - S_{wr} - S_{nr}} \qquad \text{for} \qquad Z_c < Z_{max} \tag{39}$$

The pseudo functions of relative permeability to water are obtained as:

$$\bar{k}_{rw} = \frac{\bar{S}_w - S_{wr}}{1 - S_{wr}} \qquad \text{for} \qquad \bar{S}_w \leqslant \bar{S}_{wmin} \tag{40}$$

and

$$\bar{k}_{rw} = \frac{\bar{S}_w k^*_{rw}}{1 - S_{wr} - S_{nr}} - \left[\frac{Z_T - Z_{max} + S_{wr}(Z_{max} - Z_B)}{b(1 - S_{wr} - S_{nr})}\right] k^*_{rw} + \frac{Z_T - Z_{max}}{b}$$

$$\text{for} \qquad \bar{S}_w > \bar{S}_{wmin} \tag{41}$$

where $\bar{S}_{wmin}$ is the minimum vertically averaged water saturation defined as:

$$\bar{S}_{wmin} = [(Z_T - Z_{max}) + S_{wr}(Z_{max} - Z_B)]/b \tag{42}$$

The pseudo relative permeability to NAPL is determined from:

$$\bar{k}_{rn} = \frac{\bar{S}_n - S_{nr}}{1 - S_{nr}} \qquad \text{for} \qquad \bar{S}_n \leqslant \bar{S}_{nmin} \tag{43}$$

and

$$\bar{k}_{rn} = \frac{k^*_{rn}}{1 - S_{wr} - S_{nr}} \left[1 - \bar{S}_w - \left(\frac{Z_{max} - Z_B}{b}\right) S_{nr}\right] \qquad \text{for} \qquad \bar{S}_n > \bar{S}_{nmin} \tag{44}$$

We can also write the DNAPL–water contact (interface) elevation (Z_c) in terms of saturation as:

$$Z_c = \frac{Z_T - b\bar{S}_w - S_{wr} Z_B}{1 - S_{wr}} \qquad \text{for} \qquad \bar{S}_w \leqslant \bar{S}_{wmin} \tag{45}$$

and

$$Z_c = \frac{Z_T - b\bar{S}_w - S_{nr} Z_{max} - S_{wr} Z_B}{1 - S_{wr} - S_{nr}} \qquad \text{for} \qquad \bar{S}_w > \bar{S}_{wmin} \tag{46}$$

4.3. Evaluation of k^*_{rw} and k^*_{rn}

Two parameters, k^*_{rw} and k^*_{rn}, arise from the derivation of pseudo constitutive relations of the GSVE model. These parameters correspond to the relative permeability to water at residual NAPL saturation, and the relative permeability to NAPL at residual water saturation, respectively. Subject to field data limitations, one may determine the values of k^*_{rw} and k^*_{rn} using the following estimates: $k^*_{rw} = 1 - S_{nr}$ and $k^*_{rn} = 1 - S_{wr}$, in which end values of relative permeability curves are determined using the ratio of available flow area to the total area to the phase within the porous media.

5. Numerical solution techniques

5.1. Discretization

The aquifer system is represented using an areal finite-element grid which may be a

rectangular or an orthogonal curvilinear grid depending on the geometry of the flow domain. The governing equations represented by Eq. 7 are approximated using the Galerkin procedure with modifications for incorporate upstream weighting of phase mobilities and storage matrix lumping. Time integration is performed using a fully implicit finite-difference scheme. This leads to the following system of algebraic equations:

$$[A_{IJ}^{\ell}\Phi_{\ell J}]^{t+\Delta t} + \frac{B_{II}}{\Delta t}[(b\bar{\phi}\rho_{\ell}\bar{S}_{\ell})_I^{t+\Delta t} - (b\bar{\phi}\rho_{\ell}\bar{S}_{\ell})_I^{t}] - \dot{M}_{\ell I} = 0$$

$$(\ell = \mathrm{F},\ \mathrm{D}), \qquad I = 1, 2, \ldots, n \tag{47}$$

where I and J are nodal indices ranging from 1 to n, with n being the number of nodes in the grid; superscript $t + \Delta t$ denotes the current time; Δt is the time increment, $\dot{M}_{\ell I}$ is the integrated nodal flux; and A_{IJ}^{ℓ} and B_{II} respectively are the fluid transmissivity and storage matrix elements given by:

$$A_{IJ}^{\ell} = \sum_e \int_{R^e} \left[\bar{k}_x \tau_{\ell x} \frac{\partial N_I}{\partial x}\frac{\partial N_J}{\partial x} + \bar{k}_y \tau_{\ell y} \frac{\partial N_I}{\partial y}\frac{\partial N_J}{\partial y}\right] \mathrm{d}R \tag{48a}$$

and

$$B_{II} = \sum_e \int_{R^e} N_I \mathrm{d}R \tag{48b}$$

in which R^e is the element subdomain; $\sum_e$ is the summation over all elements of the grid; and N_I's ($I = 1, 2, \ldots, n$) are basis functions.

For convenience, we have adopted the indicial summation notation:

$$A_{IJ}^{\ell}\Phi_{\ell J} \equiv \sum_J A_{IJ}^{\ell}\Phi_{\ell J} \tag{49}$$

For linear rectangular elements with nodal subscripts I and J ranging from 1 to 4, the element matrices can be readily evaluated using the influence coefficient technique (Huyakorn et al., 1984). The transmissivity matrix may be evaluated as follows:

$$A_{IJ}^{\ell}\Phi_{\ell J} = \sum_{J \in \eta_I} \tau_{\ell IJ}^{\mathrm{u}} \gamma_{IJ}(\Phi_{\ell I} - \Phi_{\ell J}) \tag{50}$$

where η_I is the set of connecting neighboring nodes of I such that A_{IJ}^{ℓ} is non-zero; $\tau_{\ell IJ}^{\mathrm{u}}$ is the upstream weighted value of the ℓ-phase mobility for the discrete flow between nodes I and J; and γ_{IJ} the transmissivity coefficient for the flow between nodes I and J.

The transmissivity coefficient can be calculated from:

$$\gamma_{IJ} = T_{xx}A_{IJ}^{x} + T_{yy}A_{IJ}^{y} \tag{51}$$

$$T_{xx} = \bar{k}_x\left(\frac{m}{L}\right) \tag{52a}$$

$$T_{yy} = \bar{k}_y\left(\frac{L}{m}\right) \tag{52b}$$

with L and m being the element dimensions in the x- and y-directions, respectively;

and A_{IJ}^{x} and A_{IJ}^{y} are the influence coefficients. If an orthogonal curvilinear grid with distorted elements is used, L and m then become the average element dimensions along the element local axes, x' and y', respectively.

The influence coefficients have been determined such that the global discretized flow equations at node I correspond to 9-point finite-element approximation or 5-point finite-difference approximation.

The diagonalized storage matrix element B_{II} is given by:

$$B_{II} = Lm/4 \tag{53}$$

The upstream spatial discretization described above is intended to supersede the early upstream weighted residual (UWR) finite-element scheme based on the asymmetric weighting functions given by Huyakorn and Pinder (1978).

5.2. Nonlinear treatment by Newton–Raphson procedure

The nonlinearity of Eq. 47 is handled using a residual-based, Newton–Raphson iterative technique. To obtain optimal behavior of the numerical solution in terms of convergence and mass balance, the primary dependent variables must be carefully selected. We elect to use a mixed (fluid potential–saturation) formulation with one fluid potential and one pseudo saturation chosen as the primary variables. Our formulation avoids the unnecessary use of the chain rule for differentiation to evaluate storage coefficients. The chain-rule application to highly nonlinear saturation–capillary head functions with steep and/or discontinuous gradients can lead to converged but non-mass-conserved numerical results. Such unacceptable behavior of the numerical solution has been clearly demonstrated by Celia et al. (1990) for single-phase unsaturated flow problems.

A brief description of the Newton–Raphson scheme used in the present model is given below [see Huyakorn and Pinder (1983) for further details]. Let R_I^{ℓ} (ℓ = F,D) denote the residual left-hand side of Eq. 47 which can be expressed in terms of primary variables, Φ_F and $\bar{S}_D$, in the form:

$$R_I^{\ell}(\Phi_{FI}, \bar{S}_{nI}) \equiv A_{IJ}^{\ell}\Phi_{\ell J} + \frac{B_{II}}{\Delta t}\Delta^t(b\bar{\phi}\rho_{\ell}\bar{S}_{\ell})_I = 0 \qquad \text{for} \qquad I = 1, 2, \ldots, n \tag{54}$$

where Δ^t is the time difference operator.

Application of the Newton–Raphson procedure to the above equations yields:

$$\frac{\partial R_I^{\mathrm{F}}}{\partial \Phi_{\mathrm{F}J}}\Delta\Phi_{\mathrm{F}J} + \frac{\partial R_I^{\mathrm{F}}}{\partial \bar{S}_{\mathrm{D}J}}\Delta\bar{S}_{\mathrm{D}J} = -(R_I^{\mathrm{F}})^k \tag{55a}$$

$$\frac{\partial R_I^{\mathrm{D}}}{\partial \Phi_{\mathrm{F}J}}\Delta\Phi_{\mathrm{F}J} + \frac{\partial R_I^{\mathrm{D}}}{\partial \bar{S}_{\mathrm{D}J}}\Delta\bar{S}_{\mathrm{D}J} = -(R_I^{D})^k \tag{55b}$$

where

$$\Delta\Phi_{\mathrm{F}J} = \Phi_{\mathrm{F}J}^{k+1} - \Phi_{\mathrm{F}J}^{k} \tag{56a}$$

$$\Delta\bar{S}_{\mathrm{D}J} = \bar{S}_{\mathrm{D}J}^{k+1} - \bar{S}_{\mathrm{D}J}^{k} \tag{56b}$$

and k and $k+1$ denote previous and current iteration levels, respectively.

Using the indicial notation and performing algebraic manipulation, a high efficient scheme for term-by-term evaluation of the Jacobian matrix can be derived. The elements of the resulting Jacobian matrix are as follows:

$$\frac{\partial R_I^{\mathrm{F}}}{\partial \Phi_{\mathrm{F}J}} = A_{IJ}^{\mathrm{F}} + \mathrm{IUNCON} \cdot \left[\Phi_{\mathrm{FL}} \frac{\partial A_{IL}^{\mathrm{F}}}{\partial \Phi_{\mathrm{F}J}} \right] + \frac{B_{II}}{\Delta t} \left[\frac{\partial (b\bar{\phi}\rho_{\mathrm{F}}\bar{S}_{\mathrm{F}})}{\partial \Phi_{\mathrm{F}}} \right]_I \delta_{IJ} \tag{57a}$$

$$\frac{\partial R_I^{\mathrm{D}}}{\partial \Phi_{\mathrm{F}J}} = A_{IJ}^{\mathrm{D}} + \mathrm{IUNCON} \cdot \left[\Phi_{\mathrm{DL}} \frac{\partial A_{IL}^{\mathrm{D}}}{\partial \Phi_{\mathrm{D}J}} \mp A_{IL}^{\mathrm{D}} \frac{\partial \bar{p}_{\mathrm{CL}}}{\partial \Phi_{\mathrm{D}J}} \right] + \frac{B_{II}}{\Delta t} \left[\frac{\partial (b\bar{\phi}\rho_{\mathrm{D}}\bar{S}_{\mathrm{D}})}{\partial \Phi_{\mathrm{D}}} \right]_I \delta_{IJ} \tag{57b}$$

$$\frac{\partial R_I^{\mathrm{F}}}{\partial \bar{S}_{\mathrm{D}J}} = \Phi_{\mathrm{FL}} \frac{\partial A_{IL}^{\mathrm{F}}}{\partial \bar{S}_{\mathrm{D}J}} + \frac{B_{II}}{\Delta t} \left[\frac{\partial (b\bar{\phi}\rho_{\mathrm{F}}\bar{S}_{\mathrm{F}})}{\partial \bar{S}_{\mathrm{D}}} \right]_I \delta_{IJ} \tag{57c}$$

$$\frac{\partial R_I^{\mathrm{D}}}{\partial \bar{S}_{\mathrm{D}J}} = \Phi_{\mathrm{DL}} \frac{\partial A_{IL}^{\mathrm{D}}}{\partial \bar{S}_{\mathrm{D}J}} \pm A_{IJ}^{\mathrm{F}} \frac{\partial \bar{p}_{\mathrm{cL}}}{\partial \bar{S}_{\mathrm{D}J}} + \frac{B_{II}}{\Delta t} \left[\frac{\partial (b\bar{\phi}\rho_{\mathrm{D}}\bar{S}_{\mathrm{D}})}{\partial \bar{S}_{\mathrm{D}}} \right]_I \delta_{IJ} \tag{57d}$$

where IUNCON is the coefficient equal to 0 and 1 for confined and unconfined aquifers, respectively; δ_{IJ} is the Kronecker delta; and $-$ and $+$ are used for LNAPL and DNAPL, respectively.

During each iteration, the linearized system of algebraic equations is solved for the nodal unknowns using a direct banded matrix solver. (Since the spatial discretization is 2-D, the direct solver is quite adequate.) The nodal values of the primary variables are then updated for the next iteration. If necessary, time-step adjustments are made to handle a convergence problem and continue the simulation. The updating of the nodal values of the unknown variables is performed using a scheme with an under-relaxation factor determined automatically and dependent upon the maximum convergence errors for the entire mesh. Details can be found in Huyakorn et al. (1992).

5.3. *Incorporation of initial and boundary conditions*

The initial conditions required to start a transient simulation are introduced by specifying the values of the primary variables at all nodes. These initial values may be derived from the information about the initial state of the system. In some instances, the initial conditions for a current simulation correspond to the final results of a previous simulation.

Boundary conditions for the multiphase flow equations may be specified in terms of nodal values of fluid potentials and mass fluxes. Prescribed flux conditions are treated simply by adding the specified nodal flux values to the right-hand side of the corresponding nodal equations. If the fluxes are dependent on the unknown potential (or head), then their partial derivatives with respect to the primary variables need to be evaluated and incorporated into the Jacobian matrix.

In practice, the flux terms of interest may include lateral fluxes due to ambient groundwater flow as well as vertical fluxes resulting from such mechanisms as groundwater recharge at the water table and leakage through aquitards, NAPL input due to

leakage, spills, or subsurface disposal, and withdrawal of NAPL and water by wells, galleries or drains.

Prescribed potential conditions are incorporated in the matrix system using a source/sink term fully implicitly, as treated in multiphase flow simulations (Forsyth, 1988). Practical examples of prescribed potential conditions include constant hydraulic heads in adjacent surface water bodies, and prescribed water and NAPL levels in trenches.

5.4. Treatment of wells

Withdrawal and injection wells may be used in the remediation of soil and groundwater contamination problems, and need to be incorporated in the numerical solution of the governing equations. We consider a common situation involving withdrawal wells operating under prescribed total volumetric production rates.

If the total volumetrical production rate, Q_T, is specified, then NAPL and water production rates are calculated by:

$$Q_n = \frac{\bar{\lambda}_n}{\bar{\lambda}_n + \bar{\lambda}_w} Q_T \tag{58}$$

and

$$Q_w = \frac{\bar{\lambda}_w}{\bar{\lambda}_n + \bar{\lambda}_w} Q_T \tag{59}$$

where $\bar{\lambda}_\ell$ is mobility of phase ℓ at the well, defined as:

$$\bar{\lambda}_\ell = \frac{\bar{k}_{r\ell}}{\mu_\ell} \tag{60}$$

where $\bar{k}_{r\ell}$ is the well pseudo relative permeability. Eqs. 58 and 59 satisfy the constraint:

$$Q_T = Q_n + Q_w \tag{61}$$

In order to treat production rates of each phase fully implicitly in the Newton–Raphson scheme, we need to define the pseudo relative permeability and their derivatives at well nodes which include partially penetrating effects.

Shown in Fig. 3 is a partially penetrating pumping well for withdrawing LNAPL. For all the possible interface elevations (Z_c) of mobile LNAPL lens and water, relative to the well open screen, the well pseudo relative permeability functions have been derived and summarized in Table 1. For DNAPL cases, a partially-penetrating pumping well is shown in Fig. 4. the corresponding well pseudo relative permeability functions are provided in Table 2. The Jacobian matrix is then modified using the above well flux equations and their derivatives, which are evaluated analytically or numerically.

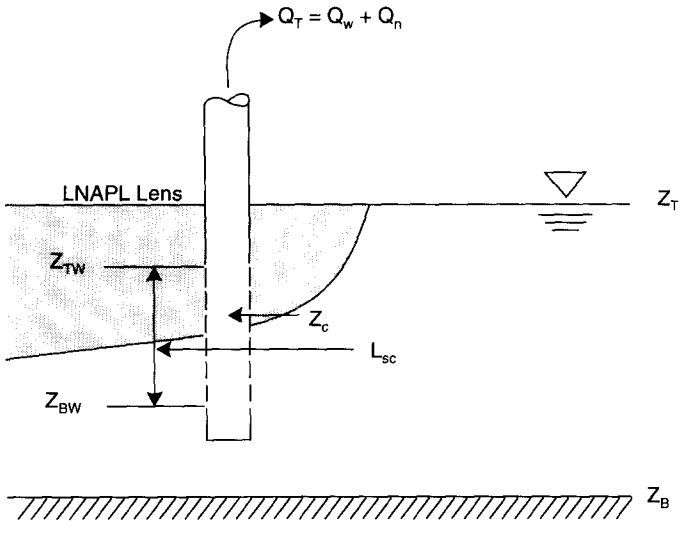

Fig. 3. A partially penetrating well through a LNAPL lens.

6. Model applicability and data requirement

The sharp-interface (GSVE) flow formulation and numerical schemes described in the foregoing sections have been implemented in a computer model designed to provide efficient analyses of NAPL contamination and remediation scenarios. In

Table 1
Well pseudo relative permeabilities and their derivations for LNAPL

Case *1*: $Z_c \geqslant Z_{TW}$

$$\bar{k}_{rn} = 0$$

$$\bar{k}_{rw} = \frac{1}{b}\begin{cases} (Z_{TW} - Z_{BW}) & (Z_{min} \geqslant Z_{TW}) \\ (Z_{TW} - Z_{min})k_{rw}^{*wn} + (Z_{min} - Z_{BW}) & (Z_{BW} < Z_{min} < Z_{TW}) \\ k_{rw}^{*wn}(Z_{TW} - Z_{BW}) & (Z_{min} \leqslant Z_{BW}) \end{cases}$$

Case *2*: $Z_{BW} < Z_c < Z_{TW}$

$$\bar{k}_{rn} = \frac{K_{rw}^{*wn}}{b}(Z_{TW} - Z_c)$$

$$\bar{k}_{rw} = \frac{1}{b}\begin{cases} (Z_c - Z_{BW}) & (Z_{min} \geqslant Z_c) \\ (Z_c - Z_{min})k_{rw}^{*wn} + (Z_{min} - Z_{BW}) & (Z_{BW} < Z_{min} < Z_c) \\ k_{rw}^{*wn}(Z_c - Z_{BW}) & (Z_{min} \leqslant Z_{BW}) \end{cases}$$

Case *3*: $Z_c \leqslant Z_{BW}$

$$\bar{k}_{rn} = \frac{k_{rn}^{*wn}}{b}(Z_{TW} - Z_{BW})$$

$$\bar{k}_{rw} = 0$$

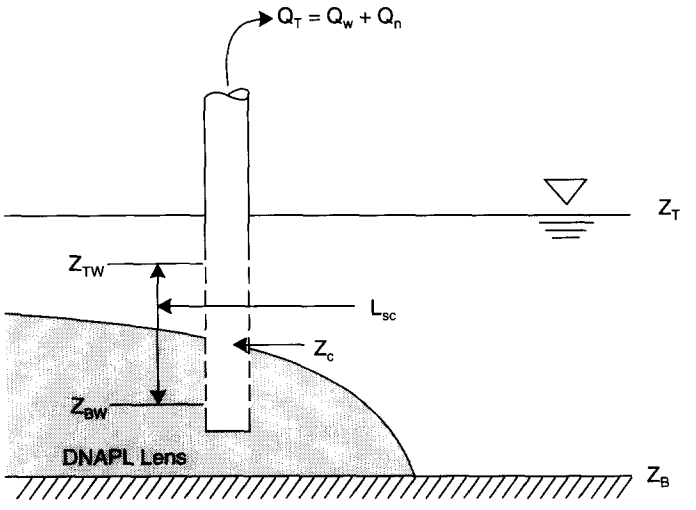

Fig. 4. A pumping well through a DNAPL lens.

practical application, the present model has several advantages over previous multiphase numerical simulators, particularly with respect to data requirement and computational performance. Owing to the use of gravity-segregated flow assumption, there is no need to provide rock or soil capillary pressure and relative permeability

Table 2
Well pseudo relative permeabilities and their derivations for DNAPL

Case *1*: $Z_c \geqslant Z_{BW}$

$$\bar{k}_{rn} = 0$$

$$\bar{k}_{rw} = \frac{1}{b}\begin{cases} (Z_{TW} - Z_{BW}) & (Z_{max} \leqslant Z_{BW}) \\ (Z_{TW} - Z_{max}) + (Z_{max} - Z_{BW})k_{rw}^{*wn} & (Z_{BW} < Z_{max} < Z_{TW}) \\ k_{rw}^{*wn}(Z_{TW} - Z_{BW}) & (Z_{max} \geqslant Z_{TW}) \end{cases}$$

Case *2*: $Z_{BW} < Z_c < Z_{TW}$

$$\bar{k}_{rn} = \frac{K_{rn}^{*wn}}{b}(Z_c - Z_{BW})$$

$$\bar{k}_{rw} = \frac{1}{b}\begin{cases} (Z_{TW} - Z_c) & (Z_{max} \leqslant Z_c) \\ (Z_{TW} - Z_{max}) + (Z_{max} - Z_c)k_{rw}^{*wn} & (Z_c < Z_{max} < Z_{Tw}) \\ k_{rw}^{*wn}(Z_{TW} - Z_c) & (Z_{max} \geqslant Z_{TW}) \end{cases}$$

Case *3*: $Z_c \geqslant Z_{TW}$

$$\bar{k}_{rn} = \frac{k_{rn}^{*wn}}{b}(Z_{TW} - Z_{BW})$$

$$\bar{k}_{rw} = 0$$

Table 3
Typical input data required for sharp-interface areal flow modeling of NAPL contamination problem

(1) Aquifer data
  (a) Intrinsic permeability (or hydraulic conductivity) and effective porosity
  (b) Base and top elevations of the aquifer layer
  (c) Residual water and NAPL saturations of aquifer material

(2) Groundwater flow parameters
  (a) Net vertical recharge and/or aquitard leakage rates
  (b) Lateral boundary conditions and/or ambient flow
  (c) Initial hydraulic head distribution

(3) NAPL data
  (a) Density and dynamic viscosity
  (b) Source locations and release rates
  (c) Initial position of NAPL–water contact (interface)

(4) Remedial system design parameters
  (a) Well coordinates and screen intervals and total withdrawal (or injection) rates
  (b) Trench locations and configurations and operating liquid levels in the individual trenches
  (c) Subsurface barrier locations and configurations

vs. saturation data in the GSVE model. Such data are usually unavailable or at best highly uncertain for a particular site. With our proposed model, a typical scenario analysis can be readily performed with limited site-specific information. Table 3 lists the types of data that would be needed for the sharp-interface modeling approach. It is understood the density and viscosity of groundwater are fixed parameters internally set by the model. Much of the listed data correspond to data normally required for a routine single-phase (fully saturated) groundwater flow simulation. The additional data pertain to simple physical properties of NAPL (density and dynamic viscosity), and source locations and release rates. The variably saturated soil properties that need to be estimated are limited to residual NAPL and water saturations. For a remediation scenario, only simple remedial design parameters and the initial location of the interface (NAPL–water contact) need to be supplied to the model.

In contrast to other available areal flow simulators (Hochmuth and Sunada, 1985; Charbenau et al., 1989; Kaluarachchi et al., 1990) which are designed to handle LNAPL scenarios only, the present model can accommodate both LNAPL and DNAPL scenarios. The use of piecewise linear pseudo constitutive relations in the sharp-interface formulation is expected to lead to improved convergence of the numerical solution and thus superior computational performance. Additionally, the proposed formulation is capable of tracking mobile and immobile (residual saturation) zones of NAPL. Such a capability is desirable to provide realistic simulations of remedial pumping scenarios and situations involving limited quantities of NAPL releases and in which further migration of soluble component plumes is of major concern.

The proposed areal simulator is based on the vertical equilibrium and gravity-segregated flow assumptions. Physically, vertical equilibrium implies uniform vertical distributions of water and NAPL potentials. The VE or near-VE condition

is frequently met in confined aquifers or the saturated zone of unconfined aquifers in which there is small or no vertical water movement. In the vadose zone, however, the vertical gradients of the fluid potentials are usually significant because of the impact of infiltration and the tendency of the NAPL to move downward toward the water table. According to Darcy's law, there is non-zero vertical potential gradient. Consequently, the VE assumption (which is essentially similar to the Dupuit–Forchheimer assumption in groundwater hydrology) may be violated. For this reason, we performed the vertical integration through the liquid-saturated thickness only, and not the entire formation thickness of the unconfined system.

In a groundwater flow system, factors which may lead to or enhance the existence vertical equilibrium (VE) include (Coats et al., 1967; Thomas, 1982): (1) high vertical permeability; (2) small thickness as compared to the scale of horizontal flow distance; (3) low areal rates of fluid movement; (4) high gravity forces and low viscous forces (i.e. low NAPL viscosity); and (5) low vertical leakage and/or recharge rates.

The gravity-segregated flow assumption implies negligible capillary forces relative to the gravity forces. This assumption should provide a reasonable good approximation when the capillary transition zone is relatively thin (say $< 10\%$) as compared to the aquifer saturated thickness. For the vertical segregation of NAPL and water to be effective, the aquifer must have sufficient vertical permeability. The GSVE assumption may become invalid when fine-grained materials are present in aquifers and effects of capillary pressure are dominant. In that case, the gravity–capillary vertical equilibrium (GCVE) concept should be used to include the capillary effects instead of the fluid-segregation approach. A GCVE numerical model that complements the present GSVE model is described in Wu et al. (1994).

To determine the validity of the GSVE assumptions for petroleum reservoirs, certain criteria have been proposed by Coats et al. (1971) based on mathematical derivation. More recently, several theoretical results have been published on analysis of the VE flow condition (Fayers and Muggeridge, 1990; Yortsos, 1991, 1992). A detailed quantitative study by Yortsos (1991) examined relative importance and effects of viscous, gravity and capillary forces on immiscible, gravity-segregated flow by using a gravity number and a capillary number. However, these criteria generally require the detailed heterogeneous properties of soils, and at best their use should be limited to the LNAPL contamination problem only. In some cases, the criteria may be inapplicable to the groundwater flow system in which vertical leakage and recharge can play an important role. Following this suggestion of Thomas (1982), we adopt the following procedure for determining the validity of the GSVE assumptions. First, cross-sectional studies of the flow system are performed using available site data and the more rigorous multiphase modeling approach. The same scenarios are then simulated in one dimension using the sharp-interface (GSVE) model. If the results compare favorably with the cross-sectional runs, one would get a good indication that the GSVE assumption are working reasonably well. The sharp-interface simulator may then be used to perform a 2-D areal analysis of the 3-D multiphase flow problem.

7. Verification and simulation examples

The sharp-interface (GSVE) formulation and numerical techniques for simulating LNAPL an DNAPL contamination problems have been implemented into a FORTRAN code. In this section, four examples are provided to demonstrate the verification and utility of the sharp-interface model. To check numerical accuracy and validate the GSVE assumptions, simulation results obtained using the sharp-interface formulation are compared with analytical solutions and rigorous multiphase numerical solutions that take into account vertical flow components.

7.1. Linear displacement of oil by water

In this example, we consider a well-known petroleum reservoir engineering problem involving linear displacement (direct line drive) of oil by a waterflood in a homogeneous formation under gravity-segregated flow conditions. The analytical solution to the problem was developed by Dake (1978) based on the concept of vertical equilibrium with gravity forces dominating the displacement process (i.e. via the incorporation of the GSVE assumptions).

The data used in our simulation correspond to that given by Dake (1978, p.383), and is also summarized in Table 4. Note that the rectangular domain for our sharp-interface areal flow model is of dimensions $L_x = 2000$ ft (609 m) and $L_y = 625$ ft (190.3 m) along the x- and y-axes, respectively. The reservoir thickness is 40 ft (12.2 m). At $x = 0$, the boundary condition for each injection well: $Q_w = 1000$ RB day^{-1})* was imposed. At $x = 2000$ ft, the production rate boundary condition ($Q_L = 1000$ RB day^{-1}) for each pumping well was imposed. The domain was discretized using a uniform rectangular grid consisting 100 elements and 202 nodes. Shown in Fig. 5 are the plots of cumulative oil recovery (expressed in terms of pore volume of the reservoir portion between injection and production wells), and typical profiles of the oil–water interface. The numerical results compare reasonably well with the analytical solution. Notably, the numerical model slightly underpredicts the cumulative recovery volume, and there is some smearing of the numerical profiles of the oil–water interfaces. The discrepancy noted may be partly due to certain boundary effects and approximations used in the analytical solution.

7.2. Migration of LNAPL *and* DNAPL *in a cross-section of unconfined aquifer*

This example is selected to verify and demonstrate application of the sharp-interface (GSVE) modeling approach to typical LNAPL and DNAPL contamination scenarios. The problem concerns an unconfined aquifer that is contaminated by a continuous release of organic chemical at a rate of 1000 kg yr^{-1} m^{-2} from a 50-m-long source as illustrated in Fig. 6. The aquifer is subject to steady infiltration at a rate of 10 cm yr^{-1}. Ambient groundwater flow is assumed to occur with hydraulic gradient of

*1 RB = 1 reservoir barrel = 5.614 ft^3 ≈ 159 L.

Table 4
Data used in the simulation of linear displacement of oil by water

Parameter	Value	Unit
Reservoir thickness, b	40	ft
Base elevation, Z_B	0	
Distance between injectors and producers, L_x	2,000	ft
Distance between injection wells, L_y	625	ft
Rate of water injection for each injection well	1,000	RB day^{-1}
Porosity, ϕ	0.18	
Intrinsic permeability, k	2	darcy
Water density, ρ_w	64.92	lb ft^{-3}
Oil density, ρ_n	50.57	lb ft^{-3}
Water viscosity, μ_w	0.5	cP
Oil viscosity, μ_n	5	cP
Residual water saturation, S_{wr}	0.2	
Residual oil saturation, S_{nr}	0.2	
Initial oil saturation, $S_n(t = 0)$	0.8	
Water relative permeability at residual oil saturation, k^*_{rw}	0.3	
Oil relative permeability at residual water saturation, k^*_{rn}	0.8	

1 ft = 0.3408 m; 1 RB = 1 reservoir barrel = 5.614 ft^3 ≈ 159 L; 1 lb ft^{-3} = 0.01602 g cm^{-3}.

1.41%. The aquifer properties are as follows: $k = 6.4 \cdot 10^{-2}$ m^2, $\phi = 0.2$, $S_{wr} = S_{nr} = 0.2$, $p_c = 0$, and the relative permeability function corresponds to those given by Faust (1985, table 4) with $k^*_{rw} = 0.6$ and $k^*_{rn} = 0.68$. Groundwater properties are: $\rho_w = 1000$ kg m^{-3} and $\mu_w = 1$ cP (10^{-3} Pa s).

Two separate scenarios involving LNAPL ($\rho_n = 900$ kg m^{-3}; $\mu_n = 0.64$ cP) and DNAPL ($\rho_n = 1600$ kg m^{-3}; $\mu_n = 1.85$ cP) were analyzed. In each case, both the sharp-interface (GSVE) simulator and the rigorous multiphase simulator (Huyakorn et al., 1992) which accounts for both horizontal and vertical flow components were used. The grid used for discretizing the cross-sectional domain of the multiphase model has grid line coordinates of 0, 56, 256, 427, 533, 600, 612, 625, 638, 650, 717, 817, 967, 1167, 1367, 1567, 1767, 1967 and 2000 m in the x-direction, and 0, 1, 2, 3, 4, 4.5, 5, 5.5, 6, 6.5, 7, 7.5, 8, 8.5, 9, 9.5 and 10 m in the vertical (z) direction. The grid used for the sharp-interface flow model is the same in the x-direction as the grid of the multiphase model, the vertical dimension being reduced via the integration using the VE concept. Saturation profiles after a 3-yr release of LNAPL are shown in Fig. 6 for both simulation approaches. The lens of the sharp-interface VE approach (shaded area), containing LNAPL saturation of 0.8, is in good agreement with the LNAPL mass distribution expressed by the saturation contours of the multiphase simulation. Saturation profiles after a 5-yr DNAPL release are shown in Fig. 7. The multiphase simulation shows the DNAPL migrating vertically down to the base of the aquifer, which substantiates the VE assumption of the sharp-interface modeling approach. The DNAPL then migrates downstream due to the ambient potential gradients in the groundwater. Since DNAPL flows straight to the bottom, an assumed redistribution of DNAPL to residual saturation in the column provides for conservative estimate of the arrival time of DNAPL at the aquifer base. The

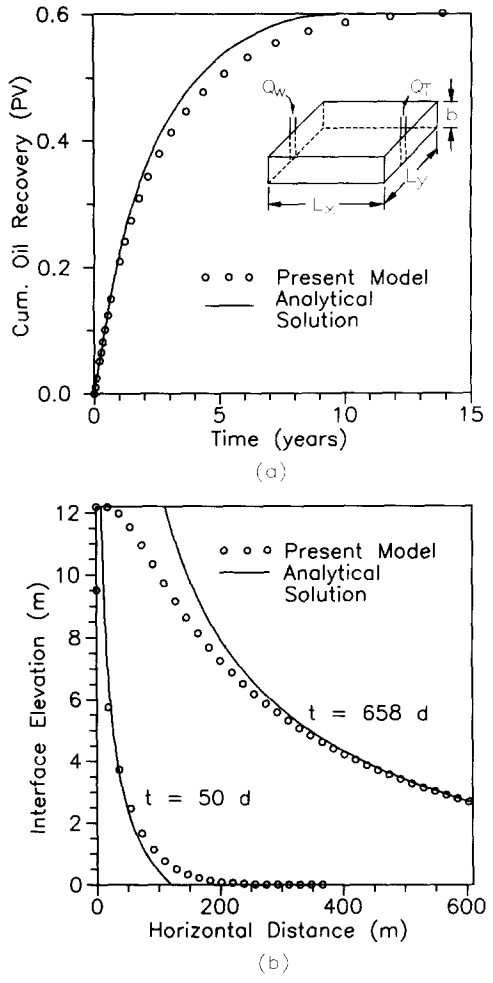

Fig. 5. Comparison of numerical and analytical solutions of linear displacement problem: (a) cumulative oil recovery vs. time; and (b) oil–water interface profiles.

agreement of the profiles of DNAPL distributions obtained from the two modeling approaches is fairly good.

7.3. Remediation of oil contamination via 5-spot well pattern

In this example, we provide another verification of the sharp-interface model and demonstrate its utility in the remedial assessment of LNAPL contamination. Specifically, the hydrocarbon recovery performance of the 5-spot well pattern shown in Fig. 8 is evaluated. Of particular concern is the upper 1-m portion of a shallow aquifer which is contaminated with oil. For the sake of simplicity in model verification, the initial conditions were specified in terms of uniform saturation distributions:

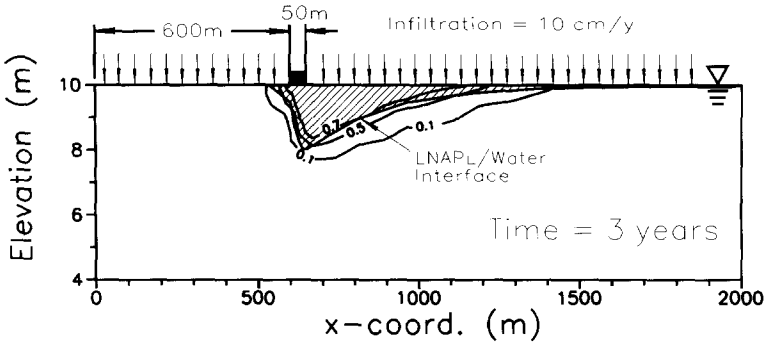

Fig. 6. Comparison of LNAPL lenses predicted by the sharp-interface and the multiphase models for the cross-sectional simulation problem.

$S_n(t = 0) = 0.8$, and $S_w(t = 0) = 0.2$. The model domain corresponds to the shaded area depicted in Fig. 8. The 5-spot waterflood problem was simulated using both the sharp-interface model and the rigorous 3-D multiphase model, NAPL3-D, which is based on the formulation described by Letniowski and Forsyth (1991). The relative permeability data were kept the same as the data used in the second example, and capillary pressure was assumed to be negligible in the 3-D multiphase simulation. The additional physical and grid data required are summarized in Table 5. Shown in the lower frame of Fig. 8 is a plot of cumulative oil recovery vs. time. As can be seen, the recovery predictions given by both models are in very good agreement. Note that the sharp-interface model slightly underpredicts the oil recovery volume over the time period of 2–4 yr. The oil–water interface locations simulated by the present model are also plotted as shown in Fig. 9. The upper frame of the figure depicts a perspective view of the oil–water interface at a late time value, whereas the lower frame depicts

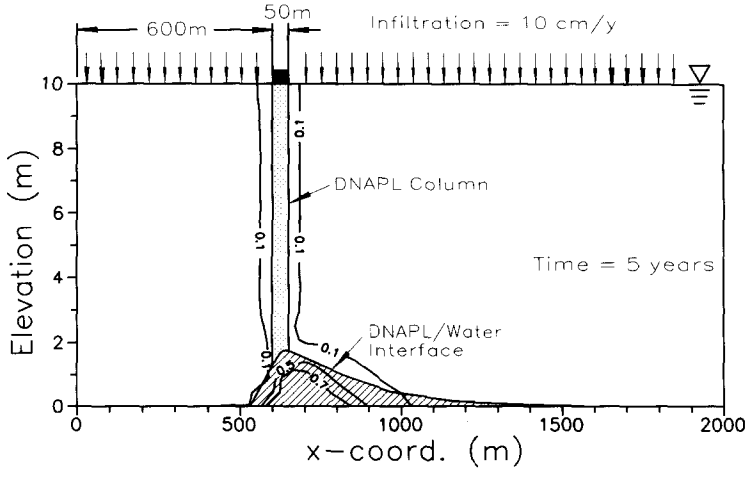

Fig. 7. Comparison of DNAPL plumes predicted by the sharp-interface and the multiphase models for the cross-sectional simulation problem.

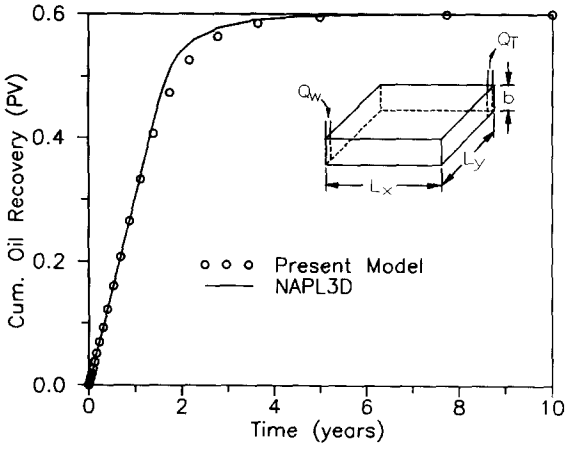

Fig. 8. Five-spot well pattern for remediation of oil contamination and predicted oil recovery.

developing profiles of the interface in a vertical cross-section passing through the selected pair of injection and production wells.

7.4. Crude-oil migration at the Bemidji site, Minnesota

In this example, we demonstrate a field application of the model by simulating the subsurface LNAPL contamination at a site near Bemidji, Minnesota. This site is

Table 5
Data used in the simulation of recovery performance of 5-spot well pattern

Parameter	Value	Unit
Water injection rate Q_w	40	$m^3\ day^{-1}\ well^{-1}$
Total liquid production rate, Q_L	40	$m^3\ day^{-1}\ well^{-1}$
Intrinsic permeability, k	10^{-12}	m^2
Porosity, ϕ	0.3	
Oil density, ρ_n	900	$kg\ m^{-3}$
Oil viscosity, μ_n	0.64	cP
Water density, ρ_w	1,000	$kg\ m^{-3}$
Water viscosity, μ_w	1	cP
Residual water saturation, S_{wr}	0.2	
Water relative permeability at residual oil saturation, k_{rw}*	0.6	
Residual oil saturation, S_{nr}	0.2	
Oil relative permeability at residual water saturation, k_{rn}*	0.68	
Grid line x-coordinates (m):		
0, 10, 20, 30, 40, 50, 60, 70, 80, 90, 100, 110, 120, 130, 140, 150, 160, 170, 180, 190, 200		
Grid line y-coordinates (m):		
0, 10, 20, 30, 40, 50, 60, 70, 80, 90, 100, 110, 120, 130, 140, 150, 160, 170, 180, 190, 200		
Grid line z-coordinates (m):		
0, 1		

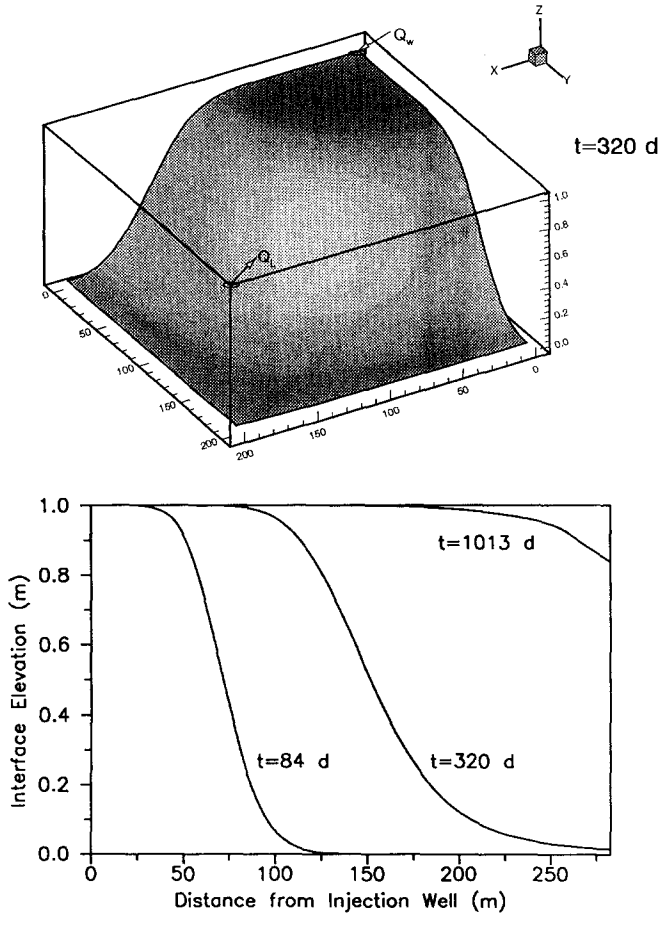

Fig. 9. Oil–water interface locations for the 5-spot well flow problem.

considered because it is a well-characterized site which has been used as a research site by the U.S. Geological Survey since 1983 (Hult, 1984) to study the mobilization, transport and fate of crude oil in the shallow subsurface.

Several field and laboratory tests have been conducted at the site to monitor the migration of the petroleum contaminants. A detailed study on measurement of the fluid-content distribution and laboratory methods was reported by Hess et al. (1992). They developed a field methodology to analyze 146 core samples retrieved from boreholes aligned along a 120-m longitudinal transect at the site (Fig. 10). The cores were collected from 7 boreholes along the transect, and a clearly defined oil lens floating on the water table was delineated for the cross-section. A previous simulation was performed along this vertical cross-section using a three-phase model with the air phase regarded as a passive phase (Essaid et al., 1991, 1993). The location of the selected cross-section (A–A') is depicted in Fig. 10. The cross-sectional profile is shown in Fig. 11 with appropriate boundary conditions. The left

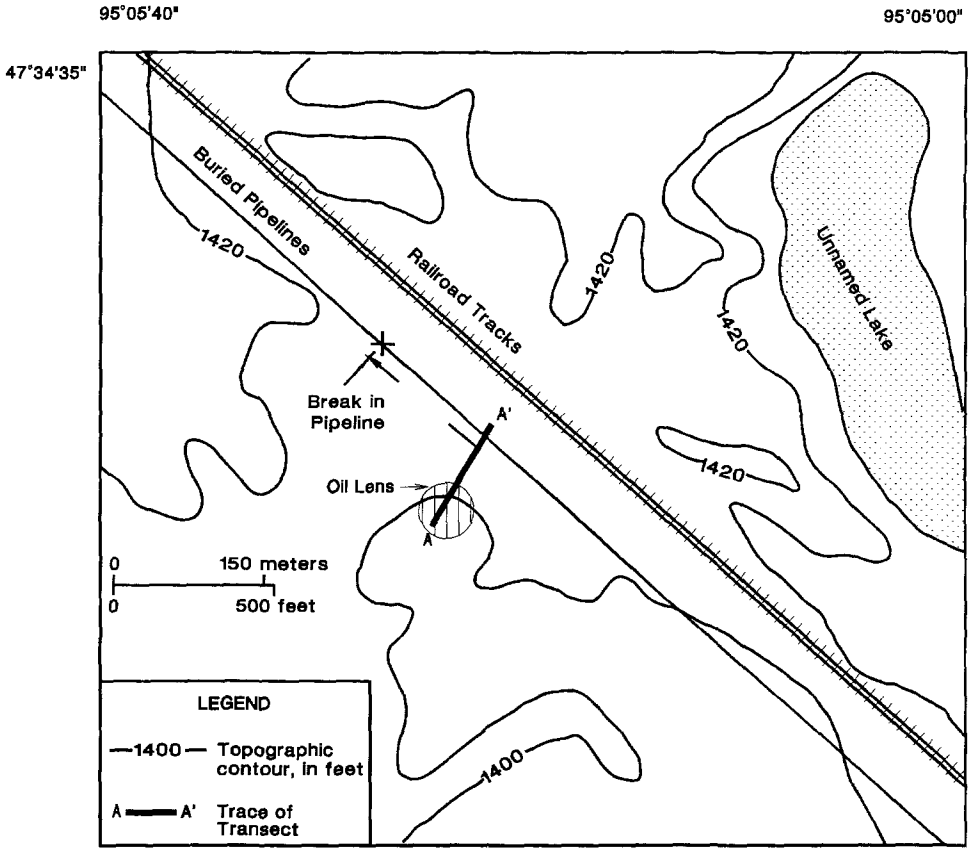

Fig. 10. Topographic map of the Bemidji study site, Minnesota (after Essaid et al., 1991).

and right vertical boundaries of the domain are treated as hydrostatic using different prescribed values of fluid potentials, Φ_w and Φ_n, which give an ambient horizontal hydraulic gradient of 0.0025 along the section. Oil is spilled across the top center of the cross-section at the rates shown in Fig. 11 for a period of 7 days. The top boundary of the section is also subject to a uniform water infiltration at a rate of 0.13 m yr^{-1}.

Shown in Table 6 are the fluid and aquifer properties, which correspond to the data provided by Baehr and Hult (1989), and Essaid et al. (1993). In the present modeling study, we simply account for the unsaturated-zone migration using a one-dimensional three-phase model (Wu et al., 1991) to simulate the downward flow from the surface source to the water table. The output of oil and water fluxes at the water table from the one-dimensional simulation was used as the source for the saturated-zone, sharp-interface simulation.

A comparison of observed and simulated profiles of the oil lens is presented in Fig. 12 for a time value of 10 yr after the spill. In terms of general configuration and extent of the lens, the model predictions and field observations are in reasonable

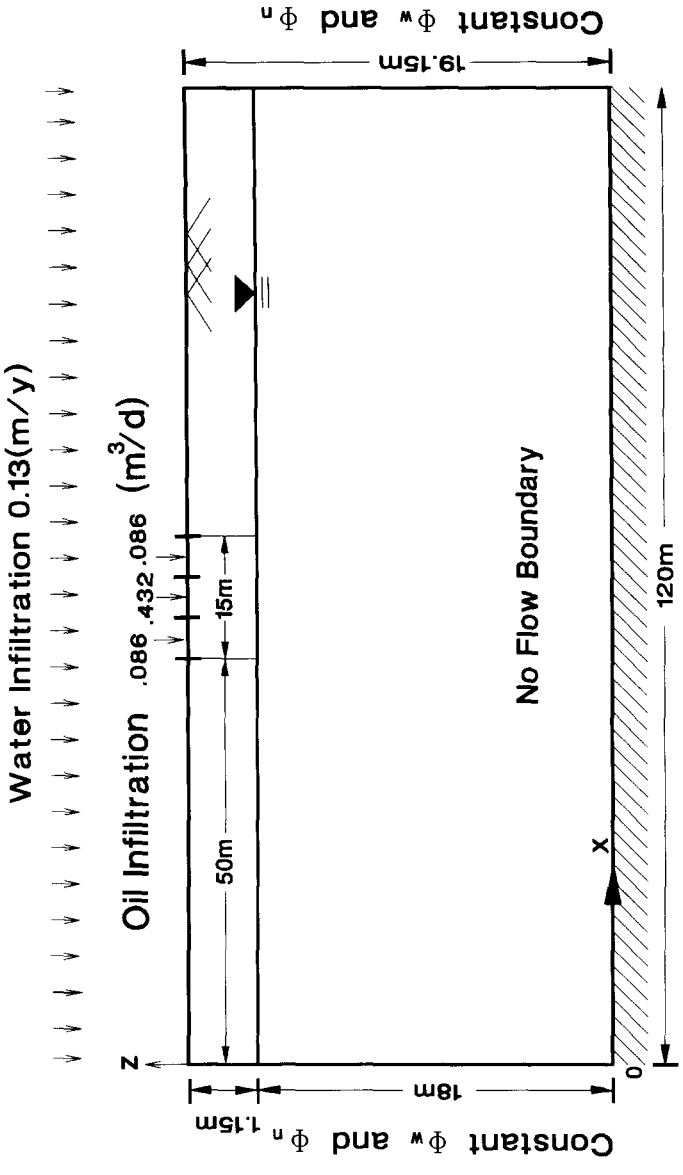

Fig. 11. Profile of the selected cross-section A–A', with the boundary conditions.

Table 6
Parameters used in the simulation of crude-oil migration at the Bemidji site, Minnesota

Parameter	Value	Unit
Horizontal permeability, k_H	$5.0 \cdot 10^{-12}$	m^2
Vertical permeability, k_v	$1.5 \cdot 10^{-11}$	m^2
Effective porosity, ϕ	0.362	
Source length, L	15	m
van Genuchten parameter, α	3.41	m^{-1}
van Genuchten index, β	2.57	
Brooks–Corey exponent, N	2.0	
Residual water saturation, S_{wr}	0.20	
Residual NAPL saturation, S_{nr}	0.05	
Water density, ρ_w	1,000	$kg\ m^{-3}$
NAPL density, ρ_n	857	$kg\ m^{-3}$
Water viscosity, μ_w	$1.139 \cdot 10^{-3}$	Pa s
NAPL viscosity, μ_n	$1.02 \cdot 10^{-2}$	Pa s
Water–air interfacial tension, σ_{aw}	0.0728	$N\ m^{-1}$
NAPL–water interfacial tension, σ_{nw}	0.0266	$N\ m^{-1}$
NAPL–air interfacial tension, σ_{an}	0.0263	$N\ m^{-1}$
Water infiltration rate, Q_w	0.13	$m\ yr^{-1}$
Cumulative NAPL injection, $\forall_n$	4.228	m^3

agreement. Irregularities of the observed oil saturation contours are due to several factors including the aquifer heterogeneity and seasonal fluctuations of the water table. The lenses predicted by the sharp-interface model agrees favorably with that predicted by the multiphase model of Essaid et al. (1993). The agreement is quite acceptable considering the limiting assumptions of the sharp-interface modeling approach. Note that the capillary effects are significant as indicated by the observed oil saturation distributions.

7.5. Mass-balance results

The mass-balance data for the four simulation samples are provided in Table 7. As can be seen from the table, the mass-balance errors of the present model are almost zero for all the cases. This is true for all the simulations we have done with the GSVE model. The mass-conservative numerical scheme, such as implemented in the present model, will guarantee good mass-balance results regardless of time step size or spatial discretization, as long as a converged solution is obtained. Table 7 also give the CPU times used for the simulations which were computed on a PC *486*/33 mHz system. A comparative study shows that the GSVE model results in two orders of magnitude savings in terms of CPU time when compared with the multiphase modeling approach.

8. Conclusions

The sharp-interface model presented herein was developed to simulate the migra-

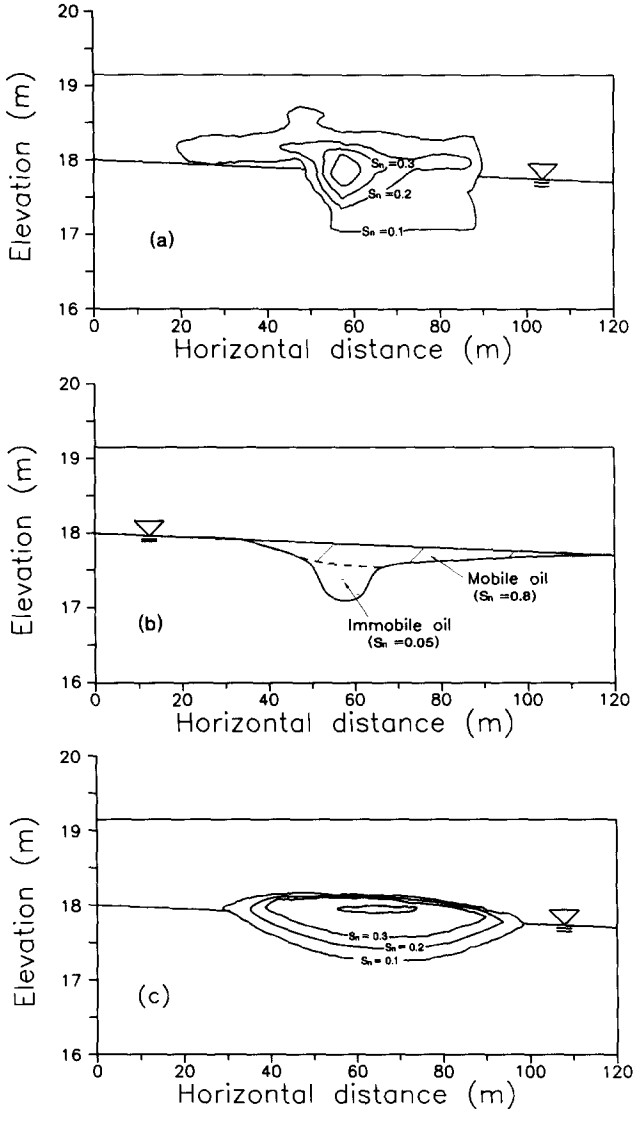

Fig. 12. Observed and simulated oil-lens configurations at elapsed time of 10 yr: (a) observed data (after Hess et al., 1992); (b) sharp-interface simulation; and (c) multiphase simulation.

tion of non-aqueous-phase liquids (NAPL's) in groundwater systems for specific application to petroleum or chemical spills and leaks and remedial design and evaluation. The model formulation incorporates the modified concept of gravity-segregated vertical equilibrium (GSVE) which yields sharp interfaces separating the zones of mobile NAPL and groundwater. As demonstrated, the present model is applicable whether the NAPL is lighter or denser that water. This is a distinct advantage over previous areal simulation models which are limited to LNAPL's.

Table 7
Mass-balance results for the four simulation examples

Example	Simulation time (yr)	CPU time[a] (s)	Mass-balance error[b]	
			NAPL	water
Linear displacement	43	58	$6.44 \cdot 10^{-8}$	$1.11 \cdot 10^{-12}$
Migration in a cross-section				
LNAPL	3	39	$5.12 \cdot 10^{-7}$	$7.02 \cdot 10^{-8}$
DNAPL	5	17	$6.56 \cdot 10^{-5}$	$6.79 \cdot 10^{-9}$
5-Spot well remediation	10	204	$1.83 \cdot 10^{-2}$	$1.34 \cdot 10^{-3}$
Bemidij site	10	10	$2.78 \cdot 10^{-4}$	$9.39 \cdot 10^{-10}$

[a]The CPU time for computation performed on a PC *486*/33 mHz.
[b]Mass-balance error is defined as:

$$\text{(mass-balance error)} = \left[\frac{\text{(mass storage change)} - \text{(net outflow)}}{|\text{(mass storage change)}|}\right] \times 100$$

The proposed model also overcomes the shortcomings of 3-D multiphase models. While the 3-D, three-phase modeling approach is the most general one, the data requirements and demand on computer resources may be excessive, especially for large-scale, 3-D field problems. The sharp-interface GSVE modeling approach has the advantages of not only reducing problem dimensions by one but also removing complex soil property data requirements (especially the need for capillary pressure and relative permeability curves). Because of these advantages the GSVE approach is potentially suitable for the following applications: (1) preliminary analyses at sites where data availability is limited; (2) large field-scale simulations which would involve an excessive number of nodal unknowns using a fully 3-D model; and (3) sensitivity analyses for which many simulations are required to assess the impacts of various hydraulic parameters.

Robust and efficient mass-conservative numerical techniques were implemented to enable practical simulations of site-specific field problems on a personal computer or workstation. Simulation examples were provided to demonstrate the model verification and utility. Both analytical and rigorous multiphase numerical solutions were used to check the results from the sharp-interface formulation. In all cases where capillary effects are mild or negligible, favorable comparisons of the different modeling approaches were achieved. The comparative simulation study indicates the adequate accuracy of the numerical schemes used and the approximation of the GSVE assumptions for the practical contamination and remediation scenarios. In performing a realistic field simulation, the CPU time required by the sharp-interface model was at least two orders of magnitude less than that required by the fully 3-D multiphase model. Such a contrast in the CPU time requirement would be even more drastic in a situation involving more highly nonlinear capillary pressure and relative permeability curves of the soil or rock material.

References

Abriola, L.M. and Pinder, G.F., 1985. A multiphase approach to the modeling of porous media contamination by organic compounds, 2. Numerical simulation. Water Resour. Res., 21: 19–26.

Aziz, K. and Settari, A., 1979. Petroleum Reservoir Simulation. Applied Science Publishers, London.

Baehr, A.L. and Hult, M.F., 1989. Determination of the air-phase permeability tensor of an unsaturated zone at the Bemidji, Minnesota, research site. Proc., U.S. Geol. Surv., Prog. on Toxic Substance Hydrology, Tech. Meet., Phoenix, AZ. U.S. Geol. Surv., Water-Invest. Rep. 88-4220.

Bear, J., 1972. Dynamics of Fluids in Porous Media. American Elsevier, New York, NY, 764 pp.

Celia, M.A., Bouloutas, E.T. and Zarba, R.L., 1990. A general mass-conservative numerical solution for the unsaturated flow equation. Water Resour. Res., 26(7): 1483–1496.

Charbenau, R.J., Wanakule, N., Chiang, C.Y., Nevin, J.P. and Klein, C.L., 1989. A two-layer model to simulate floating free product recovery: Formulation and application. Proc. Petroleum Hydrocarbons and Organic Chemicals in Groundwater: Prevention, Detection and Restoration. NWWA (Natl. Water Wells Assoc.)/API (Am. Pet. Inst.), pp. 333–345.

Coats, K.H., Nielsen, R.L., Terhune, M.H. and Weber, A.G., 1967. Simulation of three-dimensional, two-phase flow in oil and gas reservoirs. Soc. Pet. Eng. J., 7: 377–388.

Coats, K.H., Demsey, J.R. and Henderson, J.H., 1971. The use of vertical equilibrium in two-dimensional simulation of three-dimensional reservoir performance. Soc. Pet. Eng. J., 11: 63–71.

Dake, L.P., 1978. Fundamentals of Reservoir Engineering. Elsevier, Amsterdam, 444 pp.

Essaid, H.I., 1990. A multilayered sharp interface model of coupled freshwater and saltwater flow in coastal systems: Model development and application. Water Resour. Res., 26(7): 1431–1454.

Essaid, H.I., Herkelrath, W.N. and Hess, K.M., 1991. Air, oil, and water distribution at a crude-oil spill site, Bemidji, Minnesota. Proc., U.S. Geol. Surv., Prog. on Toxic Substances Hydrology, Tech. Meet., Monterey, CA. U.S. Geol. Surv., Water-Resour. Invest. Rep. 91-4034.

Essaid, H.I., Herkelrath, W.N. and Hess, K.M., 1993. Simulation of fluid distribution observed at a crude oil spill site incorporating hysteresis, oil entrapment, and spatial variability of hydraulic properties. Water Resour. Res., 29(6): 1753–1770.

Faust, C.R., 1985. Transport of immiscible fluids within and below the unsaturated zone: A numerical model. Water Resour. Res., 21(4): 587–596.

Faust, C.R., Guswa, J.H. and Mercer, J.W., 1989. Simulation of three-dimensional flow of immiscible fluids within and below the unsaturated zone. Water Resour. Res., 25(12): 2449–2464.

Fayers, F.J. and Muggeridge, A.H., 1990. Extensions to Deitz theory and behavior of gravity tongues in slightly tiled reservoirs. SPERE, pp. 487–494.

Forsyth, P.A., 1988. Simulation of nonaqueous phase groundwater contamination. Adv. Water Resour., 11: 74–83.

Forsyth, P.A., 1991. A control volume finite element approach to NAPL groundwater contamination. Soc. Ind. Appl. Math J. Sci. Comput., 12(5): 1029–1057.

Hess, K.M., Herkelrath, W.N. and Essaid, H.I., 1992. Determination of subsurface fluid contents at a crude-oil spill. J. Contam. Hydrol., 10: 75–96.

Hochmuth, D.P. and Sunada, D.K., 1985. Ground-water model of two-phase immiscible flow in coarse material. Ground Water, 23(5): 617–626.

Hult, M.F. (Editor), 1984. Ground-water contamination by crude-oil at the Bemidji, Minnesota, site: U.S. Geological Survey toxic-waste–ground-water contamination study. U.S. Geol. Surv., Water-Resour. Invest. Rep. 84-4188, 107 pp.

Huyakorn, P.S. and Pinder, G.F., 1978. New finite element technique for the solution of two-phase flow through porous media. Adv. Water Res., 2: 285–298.

Huyakorn, P.S. and Pinder, G.F., 1983. Computational Methods in Subsurface Flow. Academic Press, New York, NY, 473 pp.

Huyakorn, P.S., Thomas, S.D. and Thompson, B.M., 1984. Techniques for making finite elements competitive in modeling flow in variable saturated porous media. Water Resour. Res., 20(8): 1099–1115.

Huyakorn, P.S., Wu, Y.S., Panday, S. and Park, N.S., 1992. MAGNAS3: Multiphase analysis of

groundwater, non-aqueous phase liquid and soluble component, version 1.0. HydroGeoLogic, Inc., Herndon, VA, Code Doc. Rep.

Kaluarachchi, K. and Parker, J.C., 1989. An efficient finite element method for modeling multiphase flow. Water Resour. Res., 25: 43–44.

Kaluarachchi, K., Parker, J.C. and Lenhard, R.J., 1990. A numerical model for areal migration of water and light hydrocarbon in unconfined aquifers. Adv. Water Resour., 13(1): 29–40.

Letniowski, F. and Forsyth, P.A., 1991. A control volume finite element method for three-dimensional NAPL groundwater contamination. Int. J. Num. Meth. Fluids, 13: 1955–1970.

Martin, J.C., 1968. Partial integration of equations of multiphase flow. Pet. Eng. J., 8: 370–380.

Parker, J.C. and Lenhard, R.J., 1989. Vertical integration of three-phase flow equations for analysis of light hydrocarbon plume movement. Transport Porous Media, 5: 187–206.

Sa da Costa, A.A. and Wilson, J.L., 1979. A numerical model of seawater intrusion in aquifers. Mass. Inst. Technol., Ralph Parson Lab. Rep. No. 247, 245 pp.

Thomas, G.W., 1982. Principles of Hydrocarbon Reservoir Simulation. International Human Resources Development Corp., Boston, MA, 207 pp.

Willhite, G.P., 1986. Waterflooding. Soc. Pet. Eng. Textbook, Vol. 3, 326 pp.

Wu, Y.S., Huyakorn, P.S., Panday, S. Park, N.S. and Kool, J.B., 1991. Documentation and user's Guide: SAMFT/D-single phase and multiphase flow and transport in 1 dimension, version 2.0. Prepared for Los Alamos Natl. Lab., Los Alamos, NM.

Wu, Y.S., Huyakorn, P.S. and Park, N.S., 1994. A vertical equilibrium model for assessing NAPL contamination and remediation of groundwater systems. Water Resour. Res., 30(4): 90–912.

Yortsos, Y.C., 1991. A theoretical analysis of vertical flow equilibrium. Pap. SPE 22612, presented at 66th SPE (Soc. Pet. Eng.) Annu. Fall Meet., Dallas, TX.

Yortsos, Y.C., 1992. Analytical studies for processes at vertical equilibrium. Presented at 3rd Eur. Conf. on Mathematics of Oil Recovery, Delft Univ. Technol., Delft.